HHS Public Access

Author manuscript

J Mater Chem B. Author manuscript; available in PMC 2019 November 28.

Published in final edited form as:

J Mater Chem B. 2018 November 28; 6(44): 7247–7256. doi:10.1039/C8TB01599F.

Highly Selective, Red Emitting BODIPY-Based Fluorescent Indicators for Intracellular Mg^{2+} Imaging

Qitian Lin[a] and **Daniela Buccella**[*,a]

[a.] Department of Chemistry New York University, NY 10003, USA.

Abstract

Most fluorescent indicators for Mg^{2+} suffer from poor selectivity against other divalent cations, especially Ca^{2+}, thus do not provide reliable information on cellular Mg^{2+} concentrations in processes in which such metals are involved. We report a new set of highly selective fluorescent indicators based on alkoxystyryl-functionalized BODIPY fluorophores decorated with a 4-oxo-4*H*-quinolizine-3-carboxylic acid metal binding moiety. The new sensors, **MagQ1** and **MagQ2**, display absorption and emission maxima above 600 nm, with a 29-fold fluorescence enhancement and good quantum yields ($\Phi > 0.3$) upon coordination of Mg^{2+} in aqueous buffer. Fluorescence response to Mg^{2+} is not affected by the presence of competing divalent cations typically present in the cellular milieu, and displays minimal pH dependence in the physiologically relevant range. The choice of alkoxy groups decorating the styryl BODIPY core does not influence the basic photophysical and metal binding properties of the compounds, but has a marked effect on their intracellular retention and thus in their applicability for detection of cellular Mg^{2+} by fluorescence imaging. In particular, we demonstrate the utility of a triethyleneglycol (TEG) functionalization tactic that endows **MagQ2** with superior cellular retention in live cells by reducing active extrusion through organic anion transporters, which are thought to cause fast leakage of typical anionic dyes. With enhanced retention and excellent photophysical properties, **MagQ2** can be applied in the detection of cellular Mg^{2+} influx without interference of high concentrations of Ca^{2+} akin to those involved in signaling.

Introduction

Tightly regulated levels of Mg^{2+} within mammalian cells are essential for maintaining numerous fundamental processes including enzyme activation,[1] regulation of K^+ and Ca^{2+} ion transport[2–4] and stabilization of chromatin structure,[5] among others. Recently, Mg^{2+} was shown to act as a second messenger coupled with T-cell receptors, activating a series of intracellular effectors in lymphocytes.[6–7] To date, however, the involvement of Mg^{2+} in signaling and regulation of cellular activity remains mostly underexplored and somewhat controversial. This stands in contrast to the detailed knowledge on the role of Ca^{2+} in

[*] dbuccella@nyu.edu.

Conflicts of interest

There are no conflicts to declare.

Electronic Supplementary Information (ESI) available: supporting figures and schemes, additional experimental protocols and characterization data for new compounds. See DOI:10.1039/x0xx00000x

signaling, garnered over decades of research. The obvious disparity stems partly from the lack of sensors that can selectively detect transient changes of intracellular Mg^{2+} concentrations without interference from Ca^{2+}.

Current commercially available fluorescent probes for cellular Mg^{2+} detection, including FURAPTRA[8] (a.k.a. Mag-Fura-2)[9] and Mag-fluo-4,[9] are based on the *o*-aminophenol-*N,N,O*-triacetic acid (APTRA) metal binding group. This pentadentate chelator has been shown to form complexes with Mg^{2+} with a dissociation constant in the low millimolar range,[10] which is optimal for achieving maximum sensitivity in the detection of typical cellular concentrations of "free" or "ionized" Mg^{2+} (0.5 mM – 1.0 mM).[3] A significant drawback of APTRA, however, is the formation of tight complexes with other cations also present in biological samples, such as Ca^{2+} and Zn^{2+},[9,11–15] that may cause significant interference in Mg^{2+} detection in systems with high levels of these metals. In particular, despite being much less abundant than Mg^{2+} in the intracellular milieu, Ca^{2+} ions involved in cellular signaling can rise to concentration ranges that are orders of magnitude higher than the typical basal levels, and may fall in the detection range of the sensors.[16] Under these circumstances, APTRA-based sensors are likely to yield ambiguous results that hinder the study of Mg^{2+} in the context of Ca^{2+}-mediated signaling processes.

Seeking to alleviate the interference from Ca^{2+} in the detection of cellular Mg^{2+}, fluorescent indicators based on binding motifs with enhanced selectivity profiles have been long pursued. Farruggia *et al* reported the application of DCHQ series of fluorescent sensors, based on a diaza-18-crown-6 hydroxyquinoline motif, for the selective imaging of intracellular Mg^{2+}. These sensors display a fluorescence enhancement upon Mg^{2+} binding, whereas other metals ions such as Ca^{2+} and Zn^{2+} only induce a minor response in concentration ranges that are well above biologically relevant levels.[17] The affinity for Mg^{2+} of these sensors is quite high (K_d values of 44 and 73 μM for DCHQ1 and 2, respectively), hence they are thought to report total magnesium concentration based on their ability to outcompete natural intracellular chelators of the cation.[17–18] The groups of Oka and Suzuki adopted the 4-oxo-4*H*-quinolizine-3-carboxylic acid Mg^{2+} binding motif[19] and appended it to fluorophores such as fluorescein and rhodamine.[20–21] The resulting Mg^{2+}-selective turn-on fluorescent probes, i.e. the KMG series, have been shown to report Mg^{2+} dynamics in living cells successfully. Unfortunately, the fluorescein-based KMG 104[20] only shows modest "turn-on" ratio and low fluorescence quantum yield ($\Phi = 0.02$) upon chelation of Mg^{2+}, which requires substantial loading of the probe and yields weak signal that may be affected by interference from cellular autofluorescence. The rhodamine-based analogue KMG 301[21] displays improved fluorescence quantum yield ($\Phi = 0.15$) upon Mg^{2+} binding, but the positively charged rhodamine accumulates in mitochondria, therefore restricting the use of the probe to these organelles and precluding the detection of Mg^{2+} in other cellular compartments, including the cytosol. More recently, Kikuchi and coworkers developed a new set of fluorescent probes, namely the MGQ series, designed for the detection of intracellular Mg^{2+} with high metal selectivity.[22] The fluorescence "turn-off" response of these probes, however, is best suited for the detection of Mg^{2+} depletion and limits their general applicability. In this context, bright fluorescent indicators with high turn-on ratio and low-energy excitation, more generally applicable for detection of intracellular Mg^{2+} fluctuations, are critical but still missing tools for the study of cellular processes involving

this metal cation. In this report, we address this deficiency and introduce a new set of highly selective, red-emitting turn-on fluorescent indicators for intracellular Mg^{2+}. We illustrate their application in the detection of metal uptake in live cells, with no detectable interference from cellular Ca^{2+}, and demonstrate a triethyleneglycol (TEG) functionalization tactic for enhanced intracellular retention valuable in fluorescence microscopy imaging experiments.

Results and discussion

Design and synthesis of BODIPY-based fluorescent indicators for Mg^{2+}

Our basic indicator design is comprised of two main components, namely a 4-oxo-4*H*-quinolizine-3-carboxylic acid[19] serving as a Mg^{2+}-selective recognition motif, and a red-emitting alkoxystyryl-functionalized boron-dipyrromethene (BODIPY) fluorophore that serves as reporter and translates the binding event into a fluorescence output (**MagQ1**, Figure 1). Fluorophores of the BODIPY family are remarkable for their brightness, photostability, and low sensitivity to pH fluctuations compared to common charged dyes such as fluorescein and rhodamine, thus have become increasingly popular in the design of sensors and tags for bioimaging applications.[23–25] One other notable aspect of some BODIPY derivatives, however, is their limited water solubility and tendency to form aggregates that affect their optical properties.[26–27] To ensure sufficient water solubility of our indicator and avoid potential accumulation in cellular lipophilic compartments, charged carboxypropionyl groups were incorporated onto the 2 and 6 position of the BODIPY core.

Photoinduced electron transfer (PeT) between the metal binding group and the BODIPY fluorophore is exploited here for modulation of the fluorescent output of the indicator, endowing it with metal-sensing capabilities. Specifically, Nagano and coworkers have shown that aryl substituents at the 8 position of 1,3,5,7-tetramethyl-BODIPY fluorophores have a marked influence on the fluorescence quantum yield of the dye, acting as either oxidants or reductants of the excited BODIPY and leading to quenching of the fluorescence emission.[28–30] For our system, we anticipated that photoinduced reduction of the BODIPY by the quinolizine moiety would lead to formation of a non-emissive charge separated state resulting in low fluorescence output. Upon coordination of Mg^{2+}, the driving force for PeT should decrease due to the electron-withdrawing effect of the metal ion on the Mg^{2+}-recognition moiety, thus suppressing the quenching effect and leading to fluorescence enhancement of the indicator.[31]

Synthesis of **MagQ1** was achieved in two stages, as shown in Scheme 1. First, synthesis of BODIPY **3** was achieved via one-pot reaction starting from acid-catalyzed condensation of ethyl 1-formyl-4-oxo-4*H*-quinolizine-3-carboxylate[19] (**1**) and pyrrole **2**[32]. The resulting intermediate was immediately oxidized by 1,3-dichloro-5,6-dicyano-benzoquinone (DDQ), and the fluorophore core was completed via treatment of BF_3 OEt_2 in the presence of Hünig's base. The ester moieties in compound **3** can be hydrolyzed under basic conditions followed by neutralization to yield green-emitting BODIPY **3a**, which displays Mg^{2+} sensing capabilities of its own. Nevertheless, the limited fluorescence enhancement and very low quantum yield displayed by this compound in aqueous solution (results not shown), discouraged us from pursuing it further in the context of imaging applications. During the course of our studies, Vendrell and coworkers reported a related BODIPY compound, devoid

of the water-solubilizing carboxypropyl groups, and demonstrated similar Mg^{2+} sensing properties but only in aqueous/organic solvent mixtures.[33]

In the second stage of the synthesis, the fluorophore core of BODIPY **3** was extended via Knoevenagel condensation with aldehyde **4**, endowed with a glycol substituent to aid the water solubility of the resulting alkoxystyryl BODIPY **6**. Final sensor

MagQ1 was obtained by hydrolysis of the ester substituents under basic conditions. Similar protocol was employed for the synthesis of triethylene glycol (TEG) substituted analogue **MagQ2** (*vide infra*).

Photophysical and metal binding properties of Mg^{2+} indicators

Indicator **MagQ1**, with its styryl-functionalized BODIPY core, displays an absorption maximum at 600 nm (Figure S1) and fluorescence emission maximum at 635 nm in aqueous buffer at pH 7.0, 25 °C (Figure 2 and Table 1). The sensor is weakly fluorescent in the absence of Mg^{2+}, with a quantum yield of $\Phi = 0.01$. Addition of Mg^{2+}, on the other hand, induces a significant increase of the fluorescence intensity (29-fold increase, $\Phi = 0.35$ in the Mg^{2+} saturated form) with negligible spectral shift. These observations are consistent with a sensing mechanism involving modulation of PeT, which is expected to result in a fluorescence emission enhancement with little or no effect on the absorption profile. The photophysical properties of **MagQ1**, particularly the long wavelength excitation and emission maxima, combined with high brightness and good fluorescence enhancement for Mg^{2+} detection (summarized in Table 1), are very appealing for bioimaging applications in which reduced photodamage to the sample and minimal interference from autofluorescence are sought.

The affinity of **MagQ1** for Mg^{2+} was determined from non-linear fit of the integrated fluorescence emission of the indicator as a function of Mg^{2+} concentration (Figure 2, inset and Figure S2), using a 1:1 metal-to-indicator binding model. The K_d of the complex was found to be 1.50 ± 0.02 mM, a desirable dissociation constant to ensure optimal sensitivity for the detection of typical intracellular concentrations of this metal.

Studies by Levy and coworkers[19] have revealed that the 4-oxo-4*H*-quinolizine-3-carboxylic acid motif, which on its own is somewhat fluorescent, is insensitive to chelatable Ca^{2+} even in millimolar concentrations that far exceed typical biological levels of this cation (~100 nM[16]). We anticipated that **MagQ1** would share similar features and display good metal selectivity profile. Indeed, as shown in Figure 3A, whereas significant fluorescence enhancement is observed in the presence of a physiologically relevant concentration of Mg^{2+} (1 mM), almost no fluorescence turn-on is observed upon treatment with other divalent metal ions, including Ca^{2+} and the first row transition metal ions from Mn^{2+} to Zn^{2+} (10 μM). It should be noted that the exchangeable or chelatable pools of transition metal ions in the cellular milieu typically fall in concentration ranges that are much lower than those tested here, thus they are unlikely to induce a false fluorescence response in cellular imaging experiments. Furthermore, none of the tested metal ions, with the exception of Cu^{2+} in high concentrations, appears to interfere with the detection of Mg^{2+} in competition experiments (Figure 3B). These results indicate that **MagQ1** should be suitable for detection

of the target Mg^{2+} in the complex mixture of the cellular environment, where a variety of competing metal ions coexist.

Taking into consideration that intracellular pH varies among different subcellular compartments, ranging from ~5.0 in lysosomes[34] to ~8.0 in mitochondria[35], the effect of pH on the performance of **MagQ1** for the detection of Mg^{2+} was investigated as well. As shown in Figure 3C, in the absence of Mg^{2+}, the sensor remains weakly fluorescent over the whole pH range investigated. Treatment with the metal ion, on the other hand, leads to consistent turn on of the fluorescence emission, thus suggesting that natural pH variations among various cellular compartments will not affect the detection of Mg^{2+} with the new sensor.

Imaging of intracellular Mg^{2+} with MagQ1 in living cells

Encouraged by the optimal affinity and selectivity for Mg^{2+}, combined with excellent tolerance to intracellular pH fluctuations and high turn-on ratio of the new sensor, we proceeded to evaluate **MagQ1** for imaging Mg^{2+} in living cells. **MagQ1** is negatively charged at pH 7 due to deprotonation of the carboxylic acid groups, thus has limited ability to diffuse across the cell membrane and enter the cells (results not shown). Hence, to enable cellular loading of the sensor, the free acid was converted into the neutral acetoxymethyl (AM) ester derivative,[36] **MagQ1-AM** (Scheme S1), which is membrane permeable. Once internalized, intracellular esterases will cleave off the ester moieties, thus activating the pro-sensor for Mg^{2+} imaging. This non-invasive loading strategy has been widely used to deliver carboxylate-based fluorescent indicators into living cells, including various examples of Mg^{2+} indicators.[8,20–21,37–40]

As shown in Figure 4, **MagQ1** enables imaging of endogenous Mg^{2+} in living HeLa cells, evidenced by the strong red fluorescence emission captured with a standard Texas Red filter set in a widefield fluorescence microscope. To verify the responsiveness of the new sensor to changes in intracellular Mg^{2+} levels, we artificially induced an influx of the cation into the cells by treatment with high concentration of exogenous $MgCl_2$ and ionophore 4-bromo A23187 (Thermo Fisher Scientific). This ionophore is a non-fluorescent derivative of mobile ion-carrier A23187 (Calcimycin), which equilibrates Mg^{2+} and Ca^{2+} across the cell membrane driven by a concentration gradient of the cation.[41–43] Under these cation influx conditions, the average fluorescence signal per cell originating from **MagQ1** was significantly higher than that observed in control cells incubated either without the ionophore or in medium depleted of exogenous divalent ions (Figures 4B,C). These results confirm that the sensor is indeed responsive and able to report on changes in cellular Mg^{2+} (Figure 4C). Furthermore, the sensor is not toxic under the conditions typically employed for imaging, as demonstrated by cell viability studies conducted at concentrations up to ten-fold higher than those employed in our own imaging experiments (Figure S3).

To evaluate the potential for interference in Mg^{2+} detection caused by Ca^{2+} surges typically involved in cellular signaling, we also measured the fluorescence intensity of **MagQ1** in cells treated with a high concentration of exogenous Ca^{2+} accompanied by the 4-bromo A23187 ionophore. The average fluorescence signal per cell obtained under these conditions showed no obvious enhancement with respect to control cells (Figure S4). These results are consistent with the metal selectivity profile displayed by the sensor *in vitro*, and clearly

demonstrate the ability of **MagQ1** to sense intracellular Mg^{2+} without interference from Ca^{2+} at elevated concentrations that are most relevant to signaling processes.

Despite the outstanding photophysical properties of **MagQ1** and the encouraging results in Mg^{2+} detection *in cellulo*, an overall decrease in absolute fluorescence intensity over time was observed in all microscopy imaging experiments conducted, suggesting poor intracellular retention of the sensor under typical imaging conditions. This drawback is common for negatively charged small molecule sensors employed in cation detection,[44] which are thought to be rapidly excreted through organic anion transporters (OAT, Figure 5A).[45] For **MagQ1**, incubation at 25 °C (in the absence of a cation influx) led to loss of ~60% of the original signal over 30 min (Figures 4B and S5). Similar loss was observed upon incubation in media either supplemented with or depleted of Mg^{2+}, indicating that the decrease in signal corresponds to dye leakage and not to a turn-off due to decrease in intracellular cation concentration. In contrast, treatment of the cells with 2.5 mM probenecid (p-[dipropylsulfamoyl]benzoic acid), an inhibitor of OAT, leads to full retention of the signal over the period of observation (Figure 5B). In combination, these results imply that the loss of signal does not correspond to photobleaching of the fluorophore but instead to its extrusion from the cell, and support the notion that the main mechanism of extrusion is some form of probenecid-sensitive active transport, and not simple diffusion.

Enhancing cellular retention: development of sensor MagQ2

To address the limited intracellular retention of **MagQ1** while maintaining its attractive properties for Mg^{2+} sensing, we sought to investigate possible chemical modifications on the structure of the sensor that would possibly change the membrane permeability and interaction with biomolecules while imposing minimal electronic influence on either the metal-recognition moiety or the fluorophore. We concentrated on replacing the alkoxy substituents of the alkoxystyryl BODIPY and chose trethylene glycol (TEG) substituents, which would impart some of the attractive features of polyethylene glycol (PEG) conjugation seen in biomolecules and pharmaceuticals, such as reduction of interactions with (other) biomolecules,[46–47] while maintaining the sensor in the small molecule regime suitable for passive cellular uptake.

TEG-functionalized analogue **MagQ2** (Figure 1) was obtained by similar protocol to that developed for the synthesis of **MagQ1** (Scheme 1), replacing aldehyde **4** by TEG-substituted benzaldehyde **5** in the Knoevenagel condensation step. Compared to its predecessor **MagQ1**, the new sensor **MagQ2** inherited all the attractive photophysical properties, including low excitation energy, large turn-on ratio and high quantum yield. The compounds also display virtually identical Mg^{2+} binding and selectivity (Figures S6–9 and Table 1). In contrast, **MagQ2** (loaded as the membrane-permeable acetoxymethyl ester derivative **MagQ2-AM**) displays a significantly improved cellular retention profile compared to **MagQ1**, with 75–80% of the average fluorescence signal maintained in living HeLa cells over 30 min of incubation in normal imaging medium (Figures 6 and S10). Such difference suggests that the TEG modification on the styryl-BODIPY core offers an effective tactic for enhancing the cellular retention of the sensor by reducing the interaction with the transporters responsible for the extrusion of organic anionic dyes. Moreover, the increased retention does not have an

effect on cell viability (Figure S11), thus has an overall positive impact on the applicability of the sensor for live cell imaging purposes.

We then evaluated the fluorescence response of **MagQ2** to intracellular changes in Mg^{2+} concentration in living HeLa cells by fluorescence microscopy. An influx of Mg^{2+} was generated by the same protocols applied for the evaluation of sensor **MagQ1**, treating with exogenous $MgCl_2$ and an ionophore. As shown in Figures 6B and6C, a clear fluorescence enhancement of the sensor was captured within 5 min after the treatment, and the average fluorescence intensity per cell remained elevated compared to control samples during the 30 min period of observation. The results confirm that, like its non-TEGylated predecessor, **MagQ2** is also able to report on changes in Mg^{2+} concentration in live cells. Yet with enhanced cellular retention, this sensor offers a new, valuable tool for fluorescence microscopy applications that may help address pressing questions in magnesium biology.

Conclusions

In summary, we have developed a new set of BODIPY-based fluorescent indicators, **MagQ1** and **MagQ2**, for the detection of Mg^{2+} in live cells by fluorescence microscopy. The styryl-functionalized BODIPY core endows the new sensors with low energy excitation and emission, whereas the 4-oxo-4*H*-quinolizine-3-carboxylic acid metal binding moiety provides the molecules with strong fluorescence enhancement in response to Mg^{2+} both *in vitro* and *in cellulo*, with no interference from typical competing metal ions present in biological samples such as Ca^{2+} and Zn^{2+}.

Despite their identical photophysical and metal-binding properties, **MagQ1** and **MagQ2** present very distinct cellular retention profiles that define their applicability in microscopy imaging experiments. Specifically, we demonstrated that functionalization of the BODIPY fluorophore with triethyleneglycol groups in **MagQ2** has no significant impact on the basic photophysical and Mg^{2+} sensing properties of the compound compared to **MagQ1**, but endows it with superior retention in live cells by decreasing active extrusion that likely involves organic anion transporters. These results are significant in that they provide a first demonstration of a simple molecular functionalization strategy that alleviates a common mechanism of extrusion affecting not only many fluorescent sensors for cations, but also anionic organic dyes and drugs in general.

With low energy excitation, good Mg^{2+}-induced fluorescence enhancement and excellent metal selectivity profile, the reported sensors offer new alternatives for the study of cellular magnesium biology by fluorescence techniques, and are particularly suited for the study of this cation in systems with elevated concentrations of competing metals such as in the context of calcium signaling.

Experimental Section

General materials and Synthetic Methods

Compounds **1**[19], **2**[32] and **5**[48] and methyl 2-bromoacetate[49] were synthesized using reported procedures. All other reagents were purchased from commercial sources and used as

received. Solvents were purified and degassed by standard procedures. Analytical thin layer chromatography (TLC) was conducted on SorbTech polyester-backed 200 μm silica gel sheets. NMR spectra were acquired on Bruker Avance 400 and Avance III 600 MHz with triple resonance CTPCI-cryoprobehead spectrometers. ^{1}H NMR chemical shifts are reported in ppm relative to SiMe4 (δ = 0) and were referenced internally with respect to residual protio impurity in the solvent (δ 7.26 for $CDCl_3$, 2.05 for acetone-d_6 and 2.50 for DMSO-d_6).[50] ^{13}C NMR chemical shifts are reported in ppm relative to $SiMe_4$ (δ = 0) and were referenced internally with respect to the solvent signal (δ 77.16 for $CDCl_3$, 29.84 for acetone-d_6).[50] ^{19}F NMR chemical shifts are reported relative to $CFCl_3$ (δ = 0) and were referenced using $C_6H_5CF_3$ in CDCl3 as external standard (δ = −63.72).[51] Coupling constants are reported in Hz. High-resolution mass spectra (HRMS) were acquired on an Agilent 6224 Accurate-Mass TOF LC/MS using APCI or ESI ionization. Reverse-phased HPLC analyses were conducted on an Agilent 1260 system with UV-Vis detection, using a ZORBAX Eclipse Plus C18 reversed phase column (4.6×50 mm, 1.8 μm particle size) and a gradient of 10% to 100% acetonitrile/water (+ 0.1% trifluoroacetic acid) over 7 min. Purification of **MagQ1**, **MagQ2**, **MagQ1-AM** and **MagQ2-AM** was conducted on an Agilent 1260 system with UV-Vis detection, using a GRACE Vision HT C18 HL reverse phase column (10×150 mm, 5 μm particle size) and a gradient of 10% to 100% acetonitrile/water (+ 0.1% trifluoroacetic acid) over 22 min with a flow rate of 5 mL/min.

Synthesis of 3

A solution of **1** (0.10 g, 0.41 mmol) in a mixture of anhydrous dichloromethane (28 mL) and absolute ethanol (2 mL) was treated with **2** (0.18, 1.0 mmol) and trifluoroacetic acid (0.1 mL) under N_2 atmosphere and stirred vigorously at R.T. overnight. DDQ (0.11 g, 0.49 mmol) was added to the resulting mixture and stirring was continued for 1 h. The solvent was evaporated under reduced pressure and the residue was dissolved in 30 mL of dichloromethane, treated with diisopropylethylamine (DIPEA, 1 mL), and stirred at R.T. for 30 min. $BF_3{\cdot}OEt_2$ (1 mL) was then added and the solution was stirred for another 2 h. The resulting mixture was washed with water, followed by brine. All aqueous washes were combined and re-extracted with dichloromethane. The combined organic fractions were dried over Na_2SO_4 and evaporated under reduced pressure. The crude was purified by column chromatography (silica gel, 5:1 dichloromethane/acetone) to afford compound **3** as dark orange solid (0.17 g, 66% yield). The solid can be recrystallized from dichloromethane/hexane. ^{1}H NMR (400 MHz, $CDCl_3$, δ): 9.53 (d, ^{3}J = 7.3 Hz, 1H), 8.27 (s, 1H), 7.65–7.60 (m, 2H), 7.30–7.27 (m, 1H), 4.41 (q, ^{3}J = 7.1 Hz, 2H), 3.64 (s, 6H), 2.63–2.61 (m, 4H), 2.57 (s, 6H), 2.35–2.32 (m, 4H), 1.41 (t, ^{3}J = 7.1 Hz, 3H), 1.35 (s, 6H). ^{13}C{^{1}H} NMR (150 MHz, $CDCl_3$, δ): 173.0, 165.4, 155.8, 155.5, 144.4, 141.4, 138.7, 135.4, 134.0, 131.8, 130.3, 130.0, 123.3, 117.2, 107.5, 107.4, 61.4, 51.9, 34.3, 19.4, 14.6, 12.9, 12.5. ^{19}F NMR (376 MHz, $CDCl_3$, δ): −146.00 to −147.11 (AB quartet of quartets, δ_{FA} = −146.36, δ_{FB} = −146.75, $^{2}J_{FF}$ = 208.2 Hz, $^{1}J_{FB}$ = 32.1 Hz). HR-TOF-MS (*m/z*): $[M+H]^+$ calcd for $C_{33}H_{36}BF_2N_3O_7$, 636.2687; found 636.2698.

Synthesis of 4

A mixture of 4-hydroxy-2-methoxybenzaldehyde (0.30 g, 2 mmol) and K_2CO_3 (0.83 g, 6 mmol) was suspended in 10 mL of DMF. 2-Bromoethanol (0.21 mL, 3 mmol) was added to

the suspension and the mixture was stirred at 80 °C overnight. The resulting mixture was cooled to R.T. and filtered. The filtrate was diluted with dichloromethane and washed with water, followed by brine. The organic fraction was dried over Na_2SO_4 and evaporated. The residue was purified by column chromatography (silica gel, 4:1 dichloromethane/ethyl acetate) to afford compound **4** as a pale pink solid (0.28 g, yield 72%). ^{1}H NMR (600 MHz, $CDCl_3$, δ): 10.28 (s, 1H), 7.80 (d, ^3J = 8.6 Hz, 1H), 6.55 (dd, ^3J = 8.6 Hz, ^4J = 1.7 Hz, 1H), 6.48 (d, ^4J = 2.2 Hz, 1H), 4.16 (t, ^3J = 4.3 Hz, 2H), 4.01–3.98 (m, 2H), 3.89 (s, 3H), 2.15 (t, ^3J = 6.1 Hz, 3H). ^{13}C{^{1}H} NMR (150 MHz, $CDCl_3$, δ): 188.5, 165.3, 163.7, 130.9, 119.4, 106.3, 98.7, 69.7, 61.3, 55.8. HR-TOF-MS (*m/z*): $[M+H]^+$ calcd for $C_{10}H_{12}O_4$, 197.0808; found 197.0813.

Synthesis of 6

A mixture of **3** (50 mg, 79 μmol) and **4** (15 mg, 79 μmol) was suspended in toluene (30 mL) and treated with piperidine (0.5 mL). A few crystals of *p*-toluenesulfonic acid monohydrate were added and the suspension was refluxed overnight. The resulting mixture was cooled to R.T. and evaporated under reduced pressure. The crude was purified by column chromatography (silica gel, 2:1 to 1:1 dichloromethane/acetone) to afford **6** as a purple solid (9 mg, yield 14%). ^{1}H NMR (600 MHz, $CDCl_3$, δ): 9.54–9.53 (m, 1H), 8.29 (s, 1H), 7.70–7.60 (m, 5H), 7.30–7.27 (m, 1H), 6.57 (dd, ^3J = 8.6 Hz, ^4J = 2.3 Hz, 1H), 6.49 (d, ^4J = 2.3 Hz, 1H), 4.42 (q, ^3J = 7.1 Hz, 2H), 4.14 (t, ^3J = 4.3 Hz, 2H), 4.00 (t, ^3J = 4.6 Hz, 2H), 3.85 (s, 3H), 3.67 (s, 3H), 3.64 (s, 3H), 2.95–2.92 (s, 4H), 2.65–2.62 (m, 2H), 2.60 (s, 3H), 2.55–2.52 (m, 2H), 2.36–2.33 (m, 2H), 1.42 (t, ^3J = 7.1 Hz, 3H), 1.39 (s, 3H), 1.36 (s, 3H). ^{13}C{^{1}H} NMR (150 MHz, $CDCl_3$, δ): 173.1, 173.0, 165.4, 161.1, 159.0, 155.5, 155.3, 152.6, 144.6, 141.6, 139.1, 137.9, 135.4, 133.0, 132.4, 132.2, 131.9, 130.34, 130.25, 130.1, 128.0, 123.4, 119.7, 117.3, 117.2, 107.8, 107.5, 106.2, 99.0, 69.5, 61.6, 61.3, 55.8, 51.9, 51.8, 34.3, 33.4, 20.9, 19.4, 14.6, 13.0, 12.5, 12.3. ^{19}F NMR (376 MHz, $CDCl_3$, δ): −142.65 to −143.68 (AB quartet of quartets, δ_{FA} = −143.02, δ_{FB} = −143.32, $^2J_{FF}$= 179.9 Hz, $^1J_{FB}$= 32.7 Hz). HR-TOF-MS (*m/z*): $[M+H]^+$ calcd for $C_{43}H_{46}BF_2N_3O_{10}$, 814.3317; found 814.3314.

Synthesis of 7

A mixture of **3** (50 mg, 79 μmol) and **5** (41 mg, 94 μmol) was suspended in toluene (25 mL) and treated with piperidine (0.5 mL). A few crystals of *p*-toluenesulfonic acid monohydrate were added and the suspension was refluxed overnight. The resulting mixture was cooled to R.T. and evaporated under reduced pressure. The crude was purified by column chromatography (silica gel, 2:1 to 1:1 dichloromethane/acetone) to afford **7** as a purple solid (11 mg, yield 13%). ^{1}H NMR (600 MHz, acetone-d_6, δ): 9.48–9.47 (m, 1H), 8.27 (s, 1H), 7.97–7.94 (m, 1H), 7.76–7.67 (m, 3H), 7.64–7.62 (m, 1H), 7.56–7.53 (m, 1H), 6.72–6.70 (m, 2H), 4.31 (q, ^3J = 7.1 Hz, 2H), 4.26 (t, ^3J = 4.7 Hz, 2H), 4.23 (t, ^3J = 4.7 Hz, 2H), 3.92 (t, ^3J = 5.0 Hz, 2H), 3.86–3.84 (m, 2H), 3.69–3.66 (m, 4H), 3.62–3.57 (m, 12H), 3.54–3.53 (m, 2H), 3.49–3.47 (m, 2H), 3.42–3.41 (m, 2H), 3.29 (s, 3H), 3.23 (s, 3H), 2.98 (t, ^3J = 7.9 Hz, 2H), 2.69–2.67 (m, 2H), 2.62–2.59 (m, 5H), 2.42–2.39 (m, 2H), 1.51 (s, 3H), 1.48 (s, 3H), 1.33 (t, ^3J = 7.1 Hz, 3H). ^{13}C{^{1}H} NMR (150 MHz, acetone-d_6, δ): 173.3, 173.2, 165.7, 162.5, 159.3, 156.2, 155.3, 152.6, 145.7, 141.9, 140.1, 139.1, 137.5, 134.1, 133.7, 133.3, 132.3, 131.3, 130.9, 130.8, 128.3, 124.0, 120.0, 118.5, 118.1, 108.1, 107.3, 107.2,

100.7, 72.7, 72.6, 71.5, 71.34, 71.28, 71.23, 71.11, 71.08, 70.3, 70.2, 69.0, 68.7, 61.0, 58.80, 58.76, 51.8, 51.7, 34.5, 33.9, 21.4, 19.8, 14.7, 13.1, 12.7, 12.4. ^{19}F NMR (376 MHz, acetone-d_6, δ): −141.23 to −141.49 (q, $^1J_{FB}$ = 32.8 Hz). HR-TOF-MS (*m/z*): $[M+H]^+$ calcd for $C_{54}H_{68}BF_2N_3O_{15}$, 1048.4784; found 1048.4803.

Synthesis of MagQ1

A sample of **6** (8 mg, 9.8 μmol) was suspended in a mixture of isopropanol (0.5 mL) and water (0.5 mL). The suspension was treated with 0.5 mL of saturated aqueous $Ba(OH)_2$ solution and stirred vigorously at R.T. The reaction was monitored to completion by HPLC (~8 h). The resulting mixture was cooled in an ice bath and acidified by addition of 1 M HCl solution. The precipitate was collected via filtration and purified by preparative reversed phase HPLC to afford the product as purple solid (1.6 mg, 22% yield). ^{1}H NMR (600 MHz, DMSO-d_6, δ): 9.48 (d, ^3J = 7.2 Hz, 1H), 8.26 (s, 1H), 8.09–8.06 (m, 1H), 7.76–7.71 (m, 2H), 7.54–7.52 (m, 3H), 6.69 (dd, ^3J = 8.6 Hz, ^4J = 2.4 Hz, 1H), 6.63 (d, ^4J = 2.4 Hz, 1H), 4.07 (t, ^3J = 4.9 Hz, 2H), 3.84 (s, 3H), 3.74 (t, ^3J = 4.7 Hz, 2H), 2.80–2.77 (m, 2H), 2.53–2.52 (m, 5H), 2.43–2.38 (m, 2H), 2.29–2.26 (m, 2H), 1.31 (s, 3H), 1.28 (s, 3H). HR-TOF-MS (*m/z*): $[M-H]^+$ calcd for $C_{39}H_{38}BF_2N_3O_{10}$, 756.2546; found 756.2547.

Synthesis of MagQ2

A sample of **7** (4 mg, 3.8 μmol) was dissolved in a mixture of isopropanol (0.2 mL) and water (0.2 mL). The solution was treated with 0.2 mL of saturated aqueous $Ba(OH)_2$ solution and stirred vigorously at R.T. The reaction was monitored to completion by HPLC (~3 h). The resulting mixture cooled in an ice bath, neutralized by addition of 1 M HCl solution, and purified by preparative reversed phase HPLC to afford the product as purple solid (1.0 mg, 26% yield).^{1}H NMR (600 MHz, DMSO-d_6, δ): 9.47 (d, ^3J = 6.6 Hz, 1H), 8.26 (s, 1H), 8.05 (br, 1H), 7.73–7.69 (m, 2H), 7.59–7.51 (m, 3H), 6.70–6.68 (m, 2H), 4.19–4.17 (m, 4H), 3.81 (t, ^3J = 4.8 Hz, 2H), 3.77 (t, ^3J = 4.6 Hz, 2H), 3.61–3.58 (m, 4H), 3.56–3.50 (m, 6H), 3.48–3.46 (m, 2H), 3.44–3.43 (m, 2H), 3.37–3.35 (m, 2H), 3.24 (s, 3H), 3.17 (s, 3H), 2.80 (t, ^3J = 7.7 Hz, 2H), 2.53–2.52 (m, 5H), 2.42–2.38 (m, 2H), 2.28–2.25 (m, 2H), 1.31 (s, 3H), 1.28 (s, 3H). HR-TOF-MS (*m/z*): $[M-H]^-$ calcd for $C_{50}H_{60}BF_2N_3O_{15}$, 990.4013; found 990.3998.

General procedure for the preparation of MagQ1-AM and MagQ2-AM

Following completion of the hydrolysis of compound **6** or **7**, as described in the protocol for the preparation **MagQ1** and **MagQ2**, respectively; the reaction was neutralized by 1 M HCl aqueous solution and then lyophilized. The residue was suspended in a mixture of DMF/Acetonitrile (1:2, v/v, 120 μL/mg of **6** or **7**) and treated with K_2CO_3 powder (10 equiv), followed by addition of methyl 2-bromoacetate (15 equiv). The mixture was stirred vigorously at R.T. for 1 h, after which the reaction was complete by HPLC analysis. The resulting suspension was filtered and the filtrate was purified by preparative HPLC to afford the desired product **MagQ1-AM** (11% yield in two steps) or **MagQ2-AM** (14% yield in two steps). The product was dissolved in acetonitrile (concentration of the solutions was quantified using the molar absorptivity of compound **6** at 600 nm, ε_{600} = 62900 ± 900 $M^{-1}\cdot cm^{-1}$, measured in the same solvent at 25 °C) and the resulting solution was divided into

aliquots of 20 nmol and evaporated in a centrifugal evaporator. The solid aliquots were stored at −20 °C until use.

- **MagQ1-AM:** HR-TOF-MS (*m/z*): $[M+H]^+$ calcd for $C_{48}H_{50}BF_2N_3O_{16}$, 974.3325; found 974.3339.
- **MagQ2-AM:** HR-TOF-MS (*m/z*): $[M+H]^+$ calcd for $C_{59}H_{72}BF_2N_3O_{21}$, 1208.4792; found 1208.4793.

General Spectroscopic Methods

All aqueous solutions were prepared using de-ionized water having a resistivity of 18 MΩ.cm. Other solvents were supplied by commercial vendors and used as received. Organic buffers, high purity metal chlorides, high-purity 25% HCl, and high purity 45% KOH were purchased from Sigma Aldrich. Quantitative solutions of the sensors in their acid form were stored at −20 °C in 50 μL aliquots in DMSO, and thawed immediately before each experiment. Measurements at pH 7.0 were conducted in aqueous buffer containing 50 mM PIPES and 100 mM KCl. Buffers were treated with Chelex resin (Bio-Rad) according to the manufacturer's protocol to remove adventitious metal ions unless otherwise noted. Measurements of pH were conducted using a Mettler Toledo FE20 with glass electrode. UV-visible absorption spectra were acquired on a Cary 100 spectrophotometer using quartz cuvettes (1 cm path length). Fluorescence spectra were acquired on a QuantaMaster 40 Photon Technology International spectrofluorometer equipped with xenon lamp source, emission and excitation monochromators, excitation correction unit, and PMT detector. Emission spectra were corrected for the detector wavelength-dependent response. The excitation spectra were corrected for the wavelength-dependent lamp intensity. Measurements were conducted at 25.0 ± 0.1 °C. Fluorescence quantum yields were determined using 0.1–1.0 μM solutions of the sensor in aqueous buffer at pH 7.0, exciting at the reported excitation maxima. Solutions of cresyl violet in methanol, with a reported quantum yield of 0.66 upon excitation at 610 nm[52] were used as standards. Fluorescence emission spectra were integrated from 580 to 750 nm. Data for metal selectivity studies were collected on a FlexStation 3 Multi-Mode Microplate Reader from Molecular Devices. The sensors were excited at 600 nm and the fluorescence intensity was recorded at 635 nm.

Determination of metal dissociation constants

Fluorescence titrations with Mg^{2+} were conducted using 1 μM solutions of the sensor in aqueous buffer at pH 7.0. Magnesium was added from a 200 mM $MgCl_2$ stock solution, to cover a range of 0–30 mM $[Mg^{2+}]_t$ in the cuvette. Excess metal was employed to confirm the saturation value. Changes in fluorescence intensity were observed immediately upon mixing and were stable over time. For each titration, the metal stock solution was treated with an appropriate amount of the sensor to match the concentration in the cuvette and prevent sensor dilution throughout the experiment. Apparent K_d values for Mg^{2+} dissociation were obtained from non-linear fitting using equation S1, where F_{min} is the integrated fluorescence emission of the sensor in the absence of metal and F_{max} is the integrated fluorescence emission of the sensor at metal saturation. The approximation $[Mg^{2+}] \approx [Mg^{2+}]_t$ was made.

$$[Mg^{2+}] = K_d \frac{F - F_{\min}}{F_{\max} - F}$$

Metal selectivity studies

Metal selectivity studies were performed using 1 μM solution of sensor **MagQ1** or **MagQ2** in aqueous buffer at pH 7.0, treated with either $CaCl_2$, $MnCl_2$, $Fe(SO_4)_2$, $CoCl_2$, $NiCl_2$, $CuCl_2$, or $ZnCl_2$ in aqueous buffer for a final concentration of 10 μM M^{n+}, or 10 μM M^{n+} and 1 mM $MgCl_2$, or 10 μM M^{n+} and 100 mM $MgCl_2$. Fluorescence emission of metal-free sensors was determined with solutions of **MagQ1** or **MagQ2** treated with 10 μM EDTA to sequester adventitious metal ions. All measurements were conducted in triplicate.

General cell culture and imaging protocols

HeLa cells cells were cultured in Dulbecco's Modified Eagle Medium (DMEM) supplemented with 10% fetal bovine serum (FBS) at 37 °C in a 5% CO_2 humidified atmosphere. Cells were seeded in 35 mm glass bottom cell culture dishes (MatTek) and allowed to grow to 50–70% confluence prior to fluorescence imaging. Fluorescence imaging experiments were performed on a Leica DMI6000B inverted fluorescence microscope equipped with a Hamamatsu ORCA-Flash 4.0 CCD camera, scanning stage, high- speed filter wheel for excitation filters and a mercury metal halide external light source. A Leica Texas Red filter cube was employed for the imaging. The microscope was operated with Leica LAS AF software. Image processing for fluorescence intensity determination was performed with Metamorph 7.7.0.0 software. Briefly, images were background subtracted and a threshold was applied to define cell boundaries. Results are presented as normalized average fluorescence intensities per cell. Error bars correspond to standard deviation (SD) on the normalized average fluorescence per cell, with N = total number of cells included in the analysis. All images were processed by the same protocol and are shown in the same scale. At least two biological replicas were conducted for each experiment.

Sensor loading and fluorescence imaging

Live HeLa cells were bathed in DMEM containing 1 μM of **MagQ1-AM** or **MagQ2-AM** in 0.01% Pluronic F-127 at R.T. for 30 min. The medium was then removed and the cells were rinsed with 2 mL of DMEM, followed by incubation in fresh DMEM at R.T. for 1 h to allow deesterification of the AM esters. The medium was then removed and cells were washed twice with HHBSS (20 mM HEPES-buffered HBSS containing 0.8 mM $MgCl_2$, 1.8 mM $CaCl_2$ and 2 g/L glucose) and bathed in 1 mL HHBSS for fluorescence imaging. After an initial image was collected, an additional 1 mL of HHBSS was added to the plate on the microscope stage and fluorescence images were captured over a period of 30 min.

To rule out the effect of dye leakage vs. possible signal loss due to metal depletion, a second set of experiments was performed as described above, using HHBSS without calcium and magnesium for the final washing and imaging.

Inhibition of extrusion by active transport

Live HeLa cells were bathed in DMEM containing 1 μM of **MagQ1-AM** or **MagQ2-AM**, 0.01% Pluronic F-127, and 2.5 mM probenecid at R.T. for 30 min. The medium was then removed and the cells were rinsed with 2 mL of DMEM, followed by incubation in fresh DMEM containing 2.5 mM probenecid at R.T. for 1 h to allow deesterification of the AM esters. The medium was then removed and cells were washed twice with HHBSS (20 mM HEPES-buffered HBSS containing 0.8 mM $MgCl_2$, 1.8 mM $CaCl_2$ and 2 g/L glucose) and bathed in 2 mL HHBSS with 2.5 mM probenecid for fluorescence imaging over a period of 1 h. Control experiments were performed using similar protocol, using media without probenecid for sensor loading and fluorescence imaging, as described in the general sensor loading and fluorescence imaging section.

Response to Mg^{2+} or Ca^{2+} influx

To verify that the sensors are responsive to Mg^{2+} influx, cells were loaded with 1 μM of **MagQ1-AM** or **MagQ2-AM** as described in the general sensor loading protocol, followed by washing and initial imaging in HHBSS without Ca^{2+} and Mg^{2+}. Subsequently, 1 mL of HHBSS solution containing 10 μM of 4-bromo A23187 ionophore and 30 mM $MgCl_2$ was added to the plate while on the microscope stage, and additional fluorescence images were captured over a period of 30 min.

A similar experiment was performed using 3 mM $CaCl_2$, instead of the 30 mM $MgCl_2$, to induce a cellular influx of Ca^{2+} and study the possible interference of this ion in the detection of endogenous Mg^{2+}.

Cell viability studies

CellTiter-Glo® Luminescent Cell Viability Assay (Promega) was performed to assess the cytotoxicity of **MagQ1** and **MagQ2**.

HeLa cells plated in a white opaque 96-well plate (20,000 cells per well) were bathed in DMEM (100 μL) containing various concentrations of **MagQ1-AM** or **MagQ2-AM** (1, 5, or 10 μM) with 0.01% Pluronic F-127 at R.T. for 30 min. The medium was then removed and the cells were incubated in fresh DMEM (100 μL) at R.T. for 1 h to allow deesterification of the AM esters, as described in the general cell loading procedure above. Cells were washed and treated with CellTiter-Glo® Reagent (Promega, 100 μL) according to the manufacturer's protocol. Control experiments were performed in the same fashion, using DMSO as vehicle. Luminescence was read using a FlexStation 3 Multi-Mode Microplate Reader from Molecular Devices. Results shown are averages from eight replicas.

Supplementary Material

Refer to Web version on PubMed Central for supplementary material.

Acknowledgements

The authors thank the National Institutes of Health (R01CA217817) for financial support. The Bruker Avance 400 NMR spectrometer was acquired with support of the National Science Foundation under award number

CHE-01162222. The CPTCI-cryoprobehead was acquired through the support of the National Institute of Health S10 grant underaward number OD016343. The authors wish to thank Jessica J. Gruskos for valuable discussions.

References

1. Cowan JA, BioMetals, 2002, 15, 225. [PubMed: 12206389]
2. White RE and Hartzell HC, Biochem. Pharmacol, 1989, 38, 859. [PubMed: 2467677]
3. Romani AM, Arch. Biochem. Biophys, 2011, 512, 1. [PubMed: 21640700]
4. de Baaij JHF, Hoenderop JGJ and Bindels RJM, Physiol. Rev, 2014, 95, 1.
5. Hartwig A, Mutat. Res, 2001, 475, 113. [PubMed: 11295157]
6. Li FY, Chaigne-Delalande B, Kanellopoulou C, Davis JC, Matthews HF, Douek DC, Cohen JI, Uzel G, Su HC and Lenardo MJ, Nature, 2011, 475, 471. [PubMed: 21796205]
7. Chaigne-Delalande B, Li FY, O'Connor GM, Lukacs MJ, Jiang P, Zheng L, Shatzer A, Biancalana M, Pittaluga S, Matthews HF, Jancel TJ, Bleesing JJ, Marsh RA, Kuijpers TW, Nichols KE, Lucas CL, Nagpal S, Mehmet H, Su HC, Cohen JI, Uzel G and Lenardo MJ, Science, 2013, 341, 186. [PubMed: 23846901]
8. Raju B, Murphy E, Levy LA, Hall RD and London RE, Am. J. Physiol, 1989, 256, C540. [PubMed: 2923192]
9. Molecular Probes Handbook: A Guide to Fluorescent Probes and Labeling Technologies, Life Technologies Corporation, 2010.
10. Brady M, Piombo SD, Hu C and Buccella D, Dalton Trans, 2016, 45, 12458. [PubMed: 27430930]
11. Brady M, Piombo SD, Hu C and Buccella D, Dalton Trans, 2016, 45, 12458. [PubMed: 27430930]
12. Basaric N, Baruah M, Qin W, Metten B, Smet M, Dehaen W and Boens N, Org. Biomol. Chem, 2005, 3, 2755. [PubMed: 16032354]
13. Simons TJB, J. Biochem. Bioph. Methods, 1993, 27, 25.
14. Sensi SL, Canzoniero LMT, Yu SP, Ying HS, Koh J-Y, Kerchner GA and Choi DW, J. Neurosci, 1997, 17, 9554. [PubMed: 9391010]
15. Cheng C and Reynolds IJ, J. Neurochem, 1998, 71, 2401. [PubMed: 9832138]
16. Clapham DE, Cell, 2007, 131, 1047. [PubMed: 18083096]
17. Farruggia G, Iotti S, Prodi L, Montalti M, Zaccheroni N, Savage PB, Trapani V, Sale P and Wolf FI, J. Am. Chem. Soc, 2006, 128, 344. [PubMed: 16390164]
18. Farruggia G, Iotti S, Prodi L, Zaccheroni N, Montalti M, Savage P, Andreani G, Trapani V and Wolf F, Journal of Fluorescence, 2009, 19, 11. [PubMed: 18528748]
19. Otten PA, London RE and Levy LA, Bioconj. Chem, 2001, 12, 203.
20. Komatsu H, Iwasawa N, Citterio D, Suzuki Y, Kubota T, Tokuno K, Kitamura Y, Oka K and Suzuki K, J. Am. Chem. Soc, 2004, 126, 16353. [PubMed: 15600336]
21. Shindo Y, Fujii T, Komatsu H, Citterio D, Hotta K, Suzuki K and Oka K, PLoS One, 2011, 6, e23684. [PubMed: 21858208]
22. Matsui Y, Sadhu KK, Mizukami S and Kikuchi K, Chem. Commun, 2017, 53, 10644.
23. Loudet A and Burgess K, Chem. Rev, 2007, 107, 4891. [PubMed: 17924696]
24. Boens N, Leen V and Dehaen W, Chem. Soc. Rev, 2012, 41, 1130. [PubMed: 21796324]
25. Hinkeldey B, Schmitt A and Jung G, ChemPhysChem, 2008, 9, 2019. [PubMed: 18816535]
26. Bergström F, Mikhalyov I, Hägglöf P, Wortmann R, Ny T and Johansson LBÅ, J. Am. Chem. Soc, 2002, 124, 196. [PubMed: 11782171]
27. Mikhalyov I, Gretskaya N, Bergström F and Johansson LBÅ, PCCP, 2002, 4, 5663.
28. Gabe Y, Urano Y, Kikuchi K, Kojima H and Nagano T, J. Am. Chem. Soc, 2004, 126, 3357. [PubMed: 15012166]
29. Ueno T, Urano Y, Kojima H and Nagano T, J. Am. Chem. Soc, 2006, 128, 10640. [PubMed: 16910633]
30. Sunahara H, Urano Y, Kojima H and Nagano T, J. Am. Chem. Soc, 2007, 129, 5597. [PubMed: 17425310]
31. Lin Q, Gruskos JJ and Buccella D, Org. Biomol. Chem, 2016, 14, 11381. [PubMed: 27858038]

32. Urano Y, Asanuma D, Hama Y, Koyama Y, Barrett T, Kamiya M, Nagano T, Watanabe T, Hasegawa A, Choyke PL and Kobayashi H, Nat. Med, 2009, 15, 104. [PubMed: 19029979]
33. Treadwell R, de Moliner F, Subiros-Funosas R, Hurd T, Knox K and Vendrell M, Org. Biomol. Chem, 2018, 16, 239. [PubMed: 29256562]
34. Mindell JA, Annu. Rev. Physiol, 2012, 74, 69. [PubMed: 22335796]
35. Llopis J, McCaffery JM, Miyawaki A, Farquhar MG and Tsien RY, Proc. Natl. Acad. Sci. USA, 1998, 95, 6803. [PubMed: 9618493]
36. Tsien RY, Nature, 1981, 290, 527. [PubMed: 7219539]
37. Suzuki Y, Komatsu H, Ikeda T, Saito N, Araki S, Citterio D, Hisamoto H, Kitamura Y, Kubota T, Nakagawa J, Oka K and Suzuki K, Anal. Chem, 2002, 74, 1423. [PubMed: 11922313]
38. Afzal MS, Pitteloud J-P and Buccella D, Chem. Commun, 2014, 50, 11358.
39. Zhang G, Gruskos JJ, Afzal MS and Buccella D, Chem. Sci, 2015, 6, 6841. [PubMed: 29861926]
40. Gruskos JJ, Zhang G and Buccella D, J. Am. Chem. Soc, 2016, 138, 14639. [PubMed: 27750004]
41. Reed PW and Lardy HA, J. Biol. Chem, 1972, 247, 6970. [PubMed: 4263618]
42. Abbott BJ, Fukuda DS, Dorman DE, Occolowitz JL, Debono M and Farhner L, Antimicrob. Agents Chemother, 1979, 16, 808. [PubMed: 119484]
43. Deber CM, Tom-Kun J, Mack E and Grinstein S, Anal. Biochem, 1985, 146, 349. [PubMed: 3927770]
44. Takahashi A, Camacho P, Lechleiter JD and Herman B, Physiol. Rev, 1999, 79, 1089. [PubMed: 10508230]
45. Divirgilio F, Steinberg TH, Swanson JA and Silverstein SC, J. Immunol, 1988, 140, 915. [PubMed: 3339244]
46. Harris JM and Chess RB, Nat. Rev. Drug Discov, 2003, 2, 214. [PubMed: 12612647]
47. Roberts MJ, Bentley MD and Harris JM, Adv. Drug Del. Rev, 2012, 64, 116.
48. Nielsen CB, Johnsen M, Arnbjerg J, Pittelkow M, McIlroy SP, Ogilby PR and Jorgensen M, J. Org. Chem, 2005, 70, 7065. [PubMed: 16122224]
49. Grynkiewicz G, Poenie M and Tsien RY, J. Biol. Chem, 1985, 260, 3440. [PubMed: 3838314]
50. Fulmer GR, Miller AJM, Sherden NH, Gottlieb HE, Nudelman A, Stoltz BM, Bercaw JE and Goldberg KI, Organometallics, 2010, 29, 2176.
51. Dungan CH and Wazer JRV, Compilation of Reported F19 NMR Chemical Shifts, 1951 to Mid-1967, Wiley-Interscience, 1970.
52. Shen J and Snook RD, Chem. Phys. Lett, 1989, 155, 583.

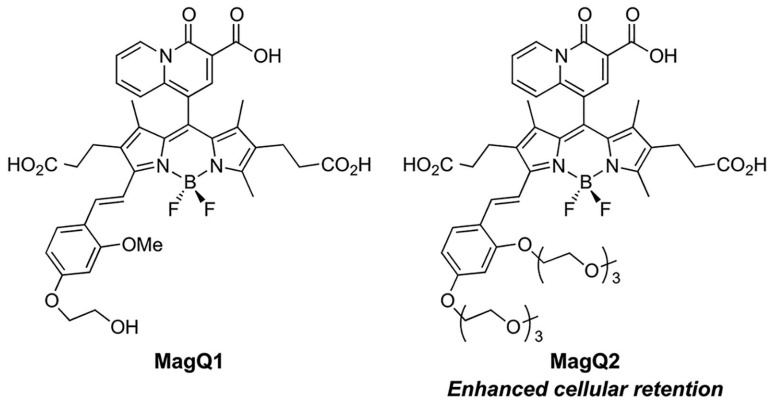

Figure 1.

Red-emitting BODIPY-based fluorescent sensors for Mg^{2+}, **MagQ1** and **MagQ2**

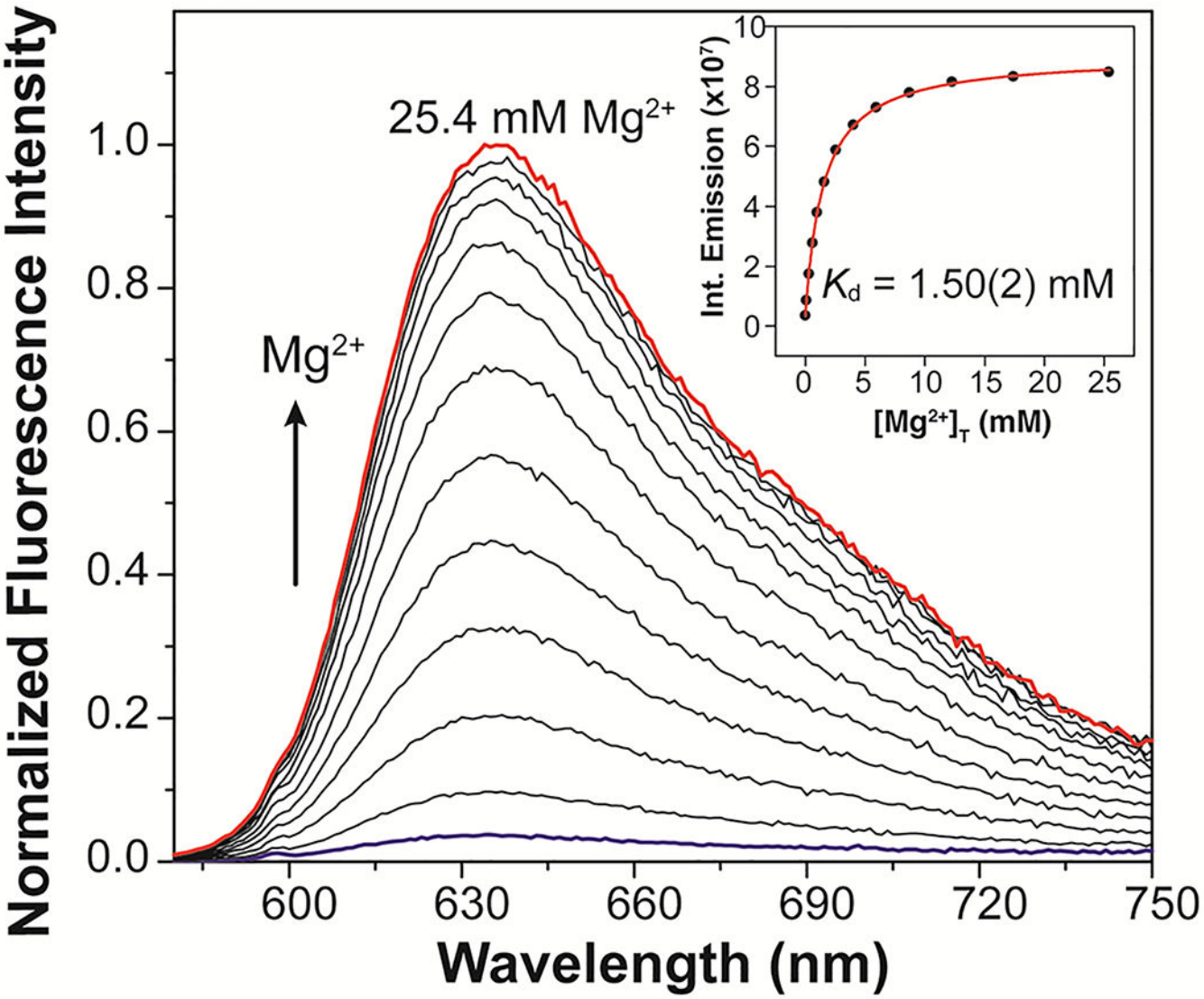

Figure 2.

Fluorescence emission spectra of a 1.0 μM solution of **MagQ1** treated with increasing concentrations of Mg^{2+}. Titration conducted in 50 mM aqueous PIPES buffer, 100 mM KCl, pH 7.0, 25 °C. Excitation wavelength λ_{ex} = 600 nm. Inset: non-linear fit (red line) of the integrated fluorescence emission (black circles) as a function of total magnesium concentration, $[Mg^{2+}]_t$, using a 1:1 metal-to-indicator binding model.

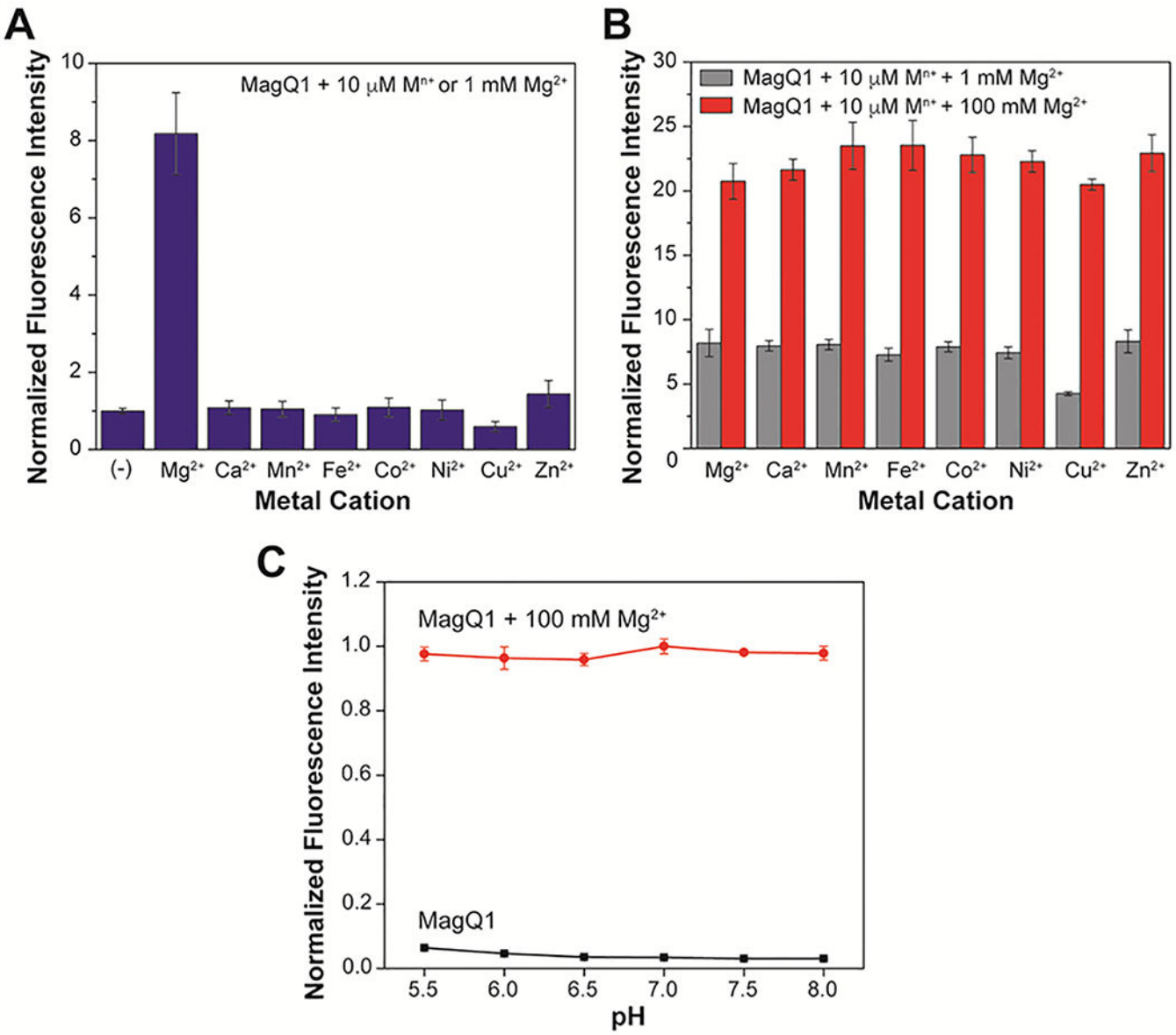

Figure 3.

(A) Fluorescence response of 1.0 μM **MagQ1** to physiological concentration of Mg^{2+} (1 mM) or to other divalent metal ions (10 μM) in aqueous buffer at 25 °C. (B) Fluorescence response of 1.0 μM **MagQ1** to 1 mM or 100 mM of Mg^{2+} in the presence of competing divalent cations, showing the selectivity of the detection in 50 mM PIPES, 100 mM KCl, pH 7.0 buffer. (C) Fluorescence emission of a 1 μM solution of **MagQ1** in aqueous buffer at pH ranging from 5.5 to 8.0 at 25 °C, in the absence (black squares) or presence (red circles) of 100 mM Mg^{2+}. Excitation wavelength λ_{ex} = 600 nm; emission wavelength λ_{em} = 635 nm. Error bars correspond to standard deviations on measurements conducted in triplicate.

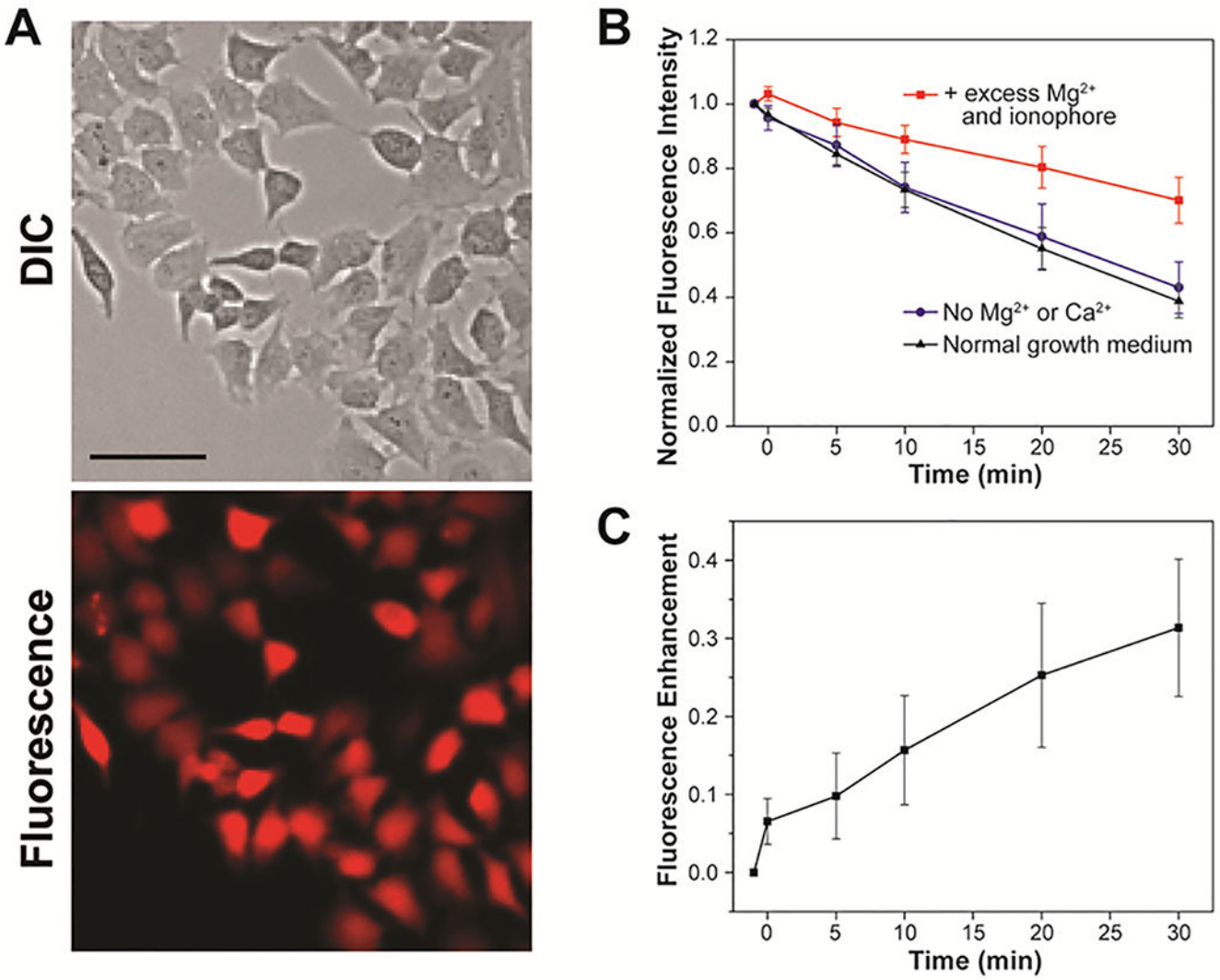

Figure 4.

(A) Representative widefield fluorescence microscopy imaging of endogenous Mg^{2+} with **MagQ1** in live HeLa cells. Scale bar = 50 μm. (B) Normalized average fluorescence per cell in samples imaged in normal growth medium (black triangles), in medium depleted from Ca^{2+} and Mg^{2+} (blue circles), and under supplementation with exogenous Mg^{2+} and ionophore (red squares). Error bars represent the SD, $N = 20$. (C) Net fluorescence enhancement caused by Mg^{2+} influx to cells treated with exogenous Mg^{2+} and ionophore. Error bars represent the SD, $N = 20$ cells.

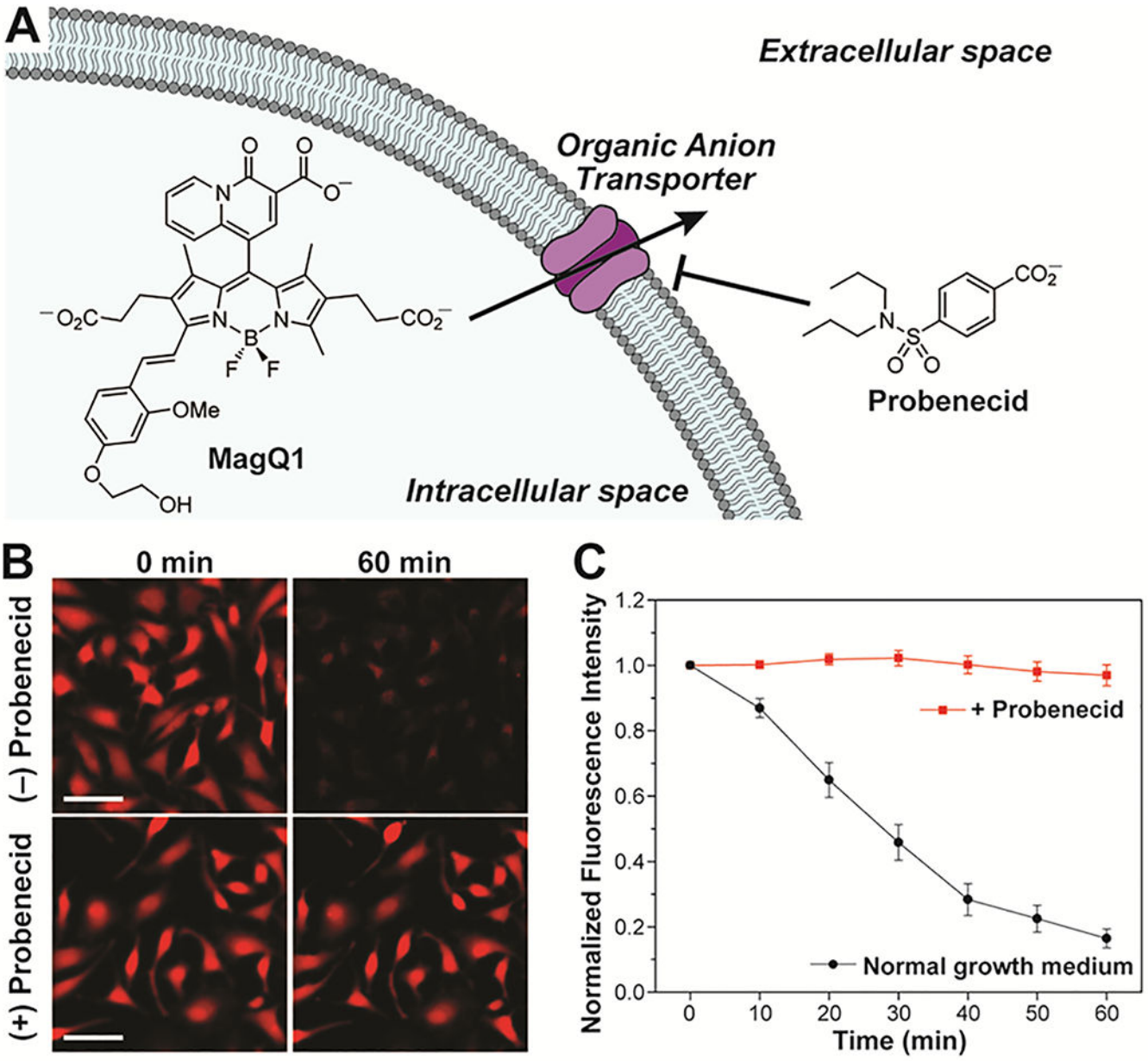

Figure 5.

(A) Possible mechanism of cellular extrusion of anionic dyes by organic anion transporters. (B) Representative widefield microscopy images of live HeLa cells stained with **MagQ1**, imaged in normal growth medium (top) or medium treated with probenecid, an OAT inhibitor (bottom). Scale bar = 50 μm. (C) Normalized average fluorescence per cell in samples stained with MagQ1, imaged in normal growth medium (black squares), and medium treated with probenecid (red circles). Error bars represent the SD, $N = 40$.

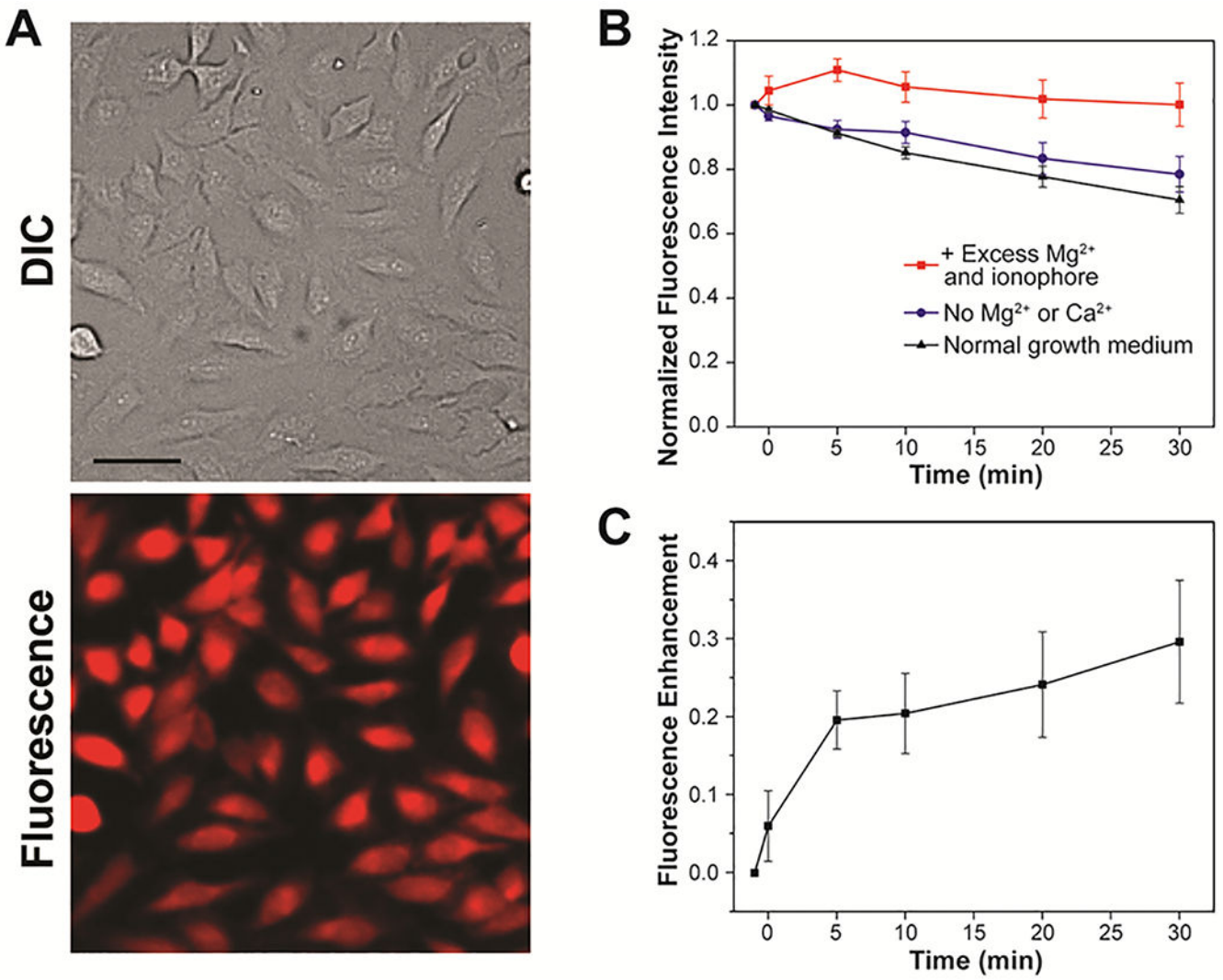

Figure 6.

(A) Representative widefield fluorescence microscopy imaging of endogenous Mg^{2+} with **MagQ2** in live HeLa cells. Scale bar = 50 μm. (B) Normalized average fluorescence per cell in samples imaged in normal growth medium (black triangles), in medium depleted from Ca^{2+} and Mg^{2+} (blue circles), and under supplementation with exogenous Mg^{2+} and ionophore (red squares). Error bars represent the SD, $N = 20$. (C) Net fluorescence enhancement caused by Mg^{2+} influx to cells treated with exogenous Mg^{2+} and ionophore. Error bars represent the SD, $N = 20$.

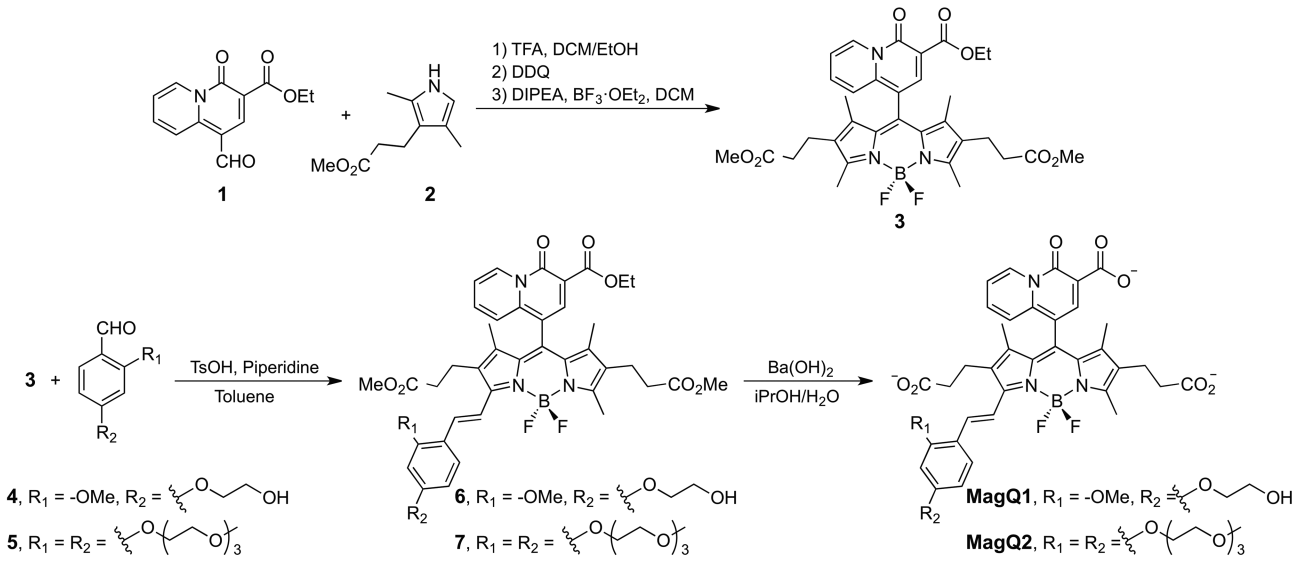

Scheme 1.
Synthesis of **MagQ1** and **MagQ2**

Table 1.

Photophysical properties of **MagQ1** and **MagQ2**[a]

Compound	λ_{abs} (nm)	λ_{exc} (nm)	λ_{em} (nm)	Φ[b]	K_d Mg^{2+}	F_{max}/F_{min}
MagQ1[c]	600[e]	600	635	0.0108(3)		
MagQ1 + Mg^{2+}[d]	602	602	636	0.35(1)	1.50(2) mM	29
MagQ2[c]	600	600	634	0.0099(8)		
MagQ2 + Mg^{2+}[d]	601	601	635	0.34(2)	1.51(5) mM	29

[a]Data collected at a probe concentration of 1 μM in aqueous buffer (50 mM PIPES, 100 mM KCl, pH 7.0, 25 °C). Excitation wavelength λ_{exc} = 600 nm. Number in parenthesis correspond to uncertainty in the last significant figure

[b]Relative quantum yield of fluorescence was determined using a cresyl violet solution in methanol as fluorescence standard (Φ = 0.66).

[c]Solution treated with 10 μM EDTA to remove adventitious metal.

[d]Solution containing 200 mM Mg^{2+}.

[e]Molar absorptivity ε = 84000 ± 1000 $M^{-1}\cdot cm^{-1}$.